Research Square

Preprints are preliminary reports that have not undergone peer review.
They should not be considered conclusive, used to inform clinical practice,
or referenced by the media as validated information.

Chlamydia-like bacterium Simkania negevensis exploits host sphingolipid salvage pathway and sphingomyelin synthesis during infection

Vera Kozjak-Pavlovic

vera.kozjak@uni-wuerzburg.de

Julius-Maximilians-University Würzburg https://orcid.org/0000-0001-9658-7018

Arpita Mohanty

Julius-Maximilians-University Würzburg

Jonas Weinrich

Julius-Maximilians-University Würzburg

Fabian Schumacher

Freie Universität Berlin https://orcid.org/0000-0001-8703-3275

Marcel Rühling

Julius-Maximilians-University Würzburg https://orcid.org/0009-0006-4757-5014

Sanisha Sunuwar

Julius-Maximilians-University Würzburg

Helena Szegedi

Julius-Maximilians-University Würzburg

Dominik Wigger

Freie Universität Berlin

Fabio Schmelz

Julius-Maximilians-Universität Würzburg

Bapin Panda

University of Osnabrück https://orcid.org/0009-0007-7984-2241

Christian Kappe

Humboldt Universität zu Berlin

Daniela Brenner

Julius-Maximilians-University Würzburg

Christoph Arenz

Humboldt University https://orcid.org/0000-0001-7613-9437

Jürgen Seibel

University of Wuerzburg https://orcid.org/0000-0002-8036-4853

Joost Holthuis

Osnabrueck University https://orcid.org/0000-0001-8912-1586

Sudip Das

Technical University Munich

Melanie Schirmer

Technical University of Munich https://orcid.org/0000-0001-6456-3679

Martin Fraunholz

Julius-Maximilians-Universität Würzburg https://orcid.org/0000-0002-4581-6244

Burkhard Kleuser

https://orcid.org/0000-0002-1888-9595

Article

Keywords: Sphingolipids, Simkania negevensis, Chlamydia, intracellular bacteria, sphingolipidomics

Posted Date: June 5th, 2026

DOI: https://doi.org/10.21203/rs.3.rs-9858454/v1

License: This work is licensed under a Creative Commons Attribution 4.0 International License.
Read Full License

Additional Declarations: There is **NO** Competing Interest.

Abstract

Simkania negevensis (Sne), a *Chlamydia*-like, obligate intracellular bacterium, forms a long-lived replicative vacuole associated with endoplasmic reticulum (ER), a major hub of sphingolipid metabolism. To understand how Sne exploits host sphingolipids, we combined sphingolipidomics, inhibitor treatment, and genetically modified cell lines to investigate infection-relevant sphingolipid profiles. Quantitative LC-MS/MS of infected cells revealed that infection skews host sphingolipid flux towards the lysosomal salvage pathway by enhancing sphingomyelin and glycosphingolipid breakdown, limiting the conversion of dihydroceramide to ceramide, and enhancing sphingosine phosphorylation. Chemical inhibition and genetic manipulation of acid sphingomyelinase or acid ceramidase significantly reduced infection rate, whereas blocking *de novo* sphingolipid synthesis or ER to Golgi ceramide transport by CERT showed no effect, confirming reliance on the salvage pathway. We show that Sne depends on sphingomyelin synthases (SMS), as SMS1/2 deletion reduced infection. Reintroduction of SMS1 or SMS2 restored infection and sphingomyelin pools. However, infected SMS1-expressing cells still displayed reduced sphingomyelin levels, implying bacteria-mediated depletion. Finally, transient reduction of plasma membrane sphingomyelin does not affect infection, indicating a critical role of internal sphingomyelin pools. These findings identify a novel relationship between *Simkania* and the host, where the lysosomal sphingolipid salvage pathway and sphingomyelin synthesis in the Golgi are leveraged for infection.

Introduction

Simkania negevensis (Sne) is a Gram-negative, obligate intracellular bacterium of the Chlamydiales order, identified in 1993 as a cell culture contaminant [1]. As an environmental *Chlamydia*, Sne can be mostly found in aquatic ecosystems, such as drinking and waste water, but also in chlorinated pool water [2, 3]. Sne is a highly adaptable microorganism, which can infect and multiply within a variety of host cells, ranging from amoeba and arthropods to mammalian epithelial and phagocytic cells [4, 5]. From the clinical point of view, Sne has been connected to respiratory diseases [6, 7], Crohn's disease [8], and lung transplant rejection [9] and it often exists as an opportunistic pathogen [10].

Similar to *Chlamydia*, Sne displays a characteristic biphasic life cycle, with two distinct forms [11]. The smaller elementary bodies (EBs) are infectious and mainly metabolically inactive, while reticulate bodies (RB) represent the metabolically active, replicative form. EBs are taken up by the host cell, where they transition into RBs and multiply within a tubular membranous compartment, termed *Simkania*-containing vacuole (SnCV), which spans the whole cell and is in close contact with the endoplasmic reticulum (ER) and mitochondria [1, 11–13]. Sne has a significantly longer life cycle than other related *Chlamydia*. The development of the SnCV peaks on day 3–4 post-infection (p.i.), but Sne-infected cells are present in culture for up to two weeks [11, 14].

The formation of the SnCV, as well as Sne survival and replication, depends on retrograde vesicular transport [15] and the acquisition of different host metabolites, such as lipids. However, details and mechanisms of Sne infection and associated metabolism are critically understudied.

Sphingolipids are major membrane constituents and are highly abundant in mammalian cells, functioning as important building blocks for the replicative compartments (inclusions) of intracellular pathogens [16]. Sphingolipids possess an amino-alcohol backbone and vary in their structure and function, which not only includes the formation of membrane microdomains, the so-called lipid rafts [17], but also signaling and regulation of apoptosis and autophagy [18, 19]. The central molecule in the sphingolipid metabolism is ceramide (Cer), which is produced through *de novo* synthesis in the ER, or through the salvage pathway, which in part takes place in lysosomes [20]. Cer is transported from the ER to the Golgi primarily through non-vesicular transport by ceramide transfer protein (CERT) [21]. The Golgi, as well as the plasma membrane (PM), contain sphingomyelin synthase (SMS) 1 and 2, respectively, which synthesize sphingomyelin (SM) from Cer [22]. On the other hand, SM and Cer can be hydrolyzed by sphingomyelinases and ceramidases, ultimately generating sphingosine-1-phosphate (S1P), which is degraded to hexadecenal and phosphoethanolamine by S1P-lyase [20].

Acquisition of host sphingolipids by related human pathogens *Chlamydia trachomatis* (Ctr) and *C. pneumoniae* (Cpn) has been extensively studied. Both possess inclusion membrane proteins (Inc), among which IncD recruits CERT, its binding partner Golgi-specific brefeldin A-resistance guanine nucleotide exchange factor 1 (GBF1), and consecutively other constituents of the SM synthesis pathway, like SMS1/2, redirecting SM biosynthesis to the inclusion [23]. Lipid acquisition by Ctr is further aided through the fragmentation of the Golgi into mini stacks [24]. Ctr, Cpn, as well as *C. psittaci* inclusions have been shown to interact with a subset of sphingomyelin-containing exocytic vesicles to acquire sphingolipids [25–27] and Sne has been reported to depend on retrograde transport for obtaining ceramide [15]. However, the morphology and close contact of the SnCV with the ER mean that Sne might possess a unique way of lipid acquisition, which we aimed to explore.

In this study, we combine infection experiments, treatment with sphingolipid biosynthesis inhibitors, genetic manipulation of host cells, and targeted LC-MS sphingolipidome analysis to understand the connection between Sne infection and sphingolipid metabolism. We show that Sne infection triggers changes in the sphingolipid profile marked by a decrease in SM and Cer and an increase in S1P. Infection studies upon loss of function in enzymes of the sphingolipid biosynthesis pathways demonstrate a dependence of Sne on the salvage pathway, with the crucial role of acid sphingomyelinase (ASM) and acid ceramidase (AC). Unlike in other *Chlamydia*, Sne infection does not depend on the *de novo* synthesis of sphingolipids or non-vesicular ceramide transport by CERT. Finally, we show that the absence of SMS1 and 2 severely impairs Sne infection, whereas reintroduction of these enzymes reveals a crucial dependence on the Golgi-derived SM and the resident SMS1 enzyme. Altogether, this study gives a novel and systematic insight into the alterations in sphingolipid profile during infection with a unique intracellular pathogen, revealing a fine balance between sphingolipid biosynthesis and content in different cell compartments and the ability of bacteria to establish a replicative niche.

Results

Simkania negevensis infection drives cell type-specific sphingolipid remodeling

To determine whether Sne infection affects sphingolipid composition of infected cells, we performed targeted lipidomics by tandem LC-MS/MS on organic solvent-extracted lipid fractions from uninfected and infected HeLa and human umbilical vein endothelial (HUVEC) cells (Fig. 1, **Supp.** Figure 1). We quantified sphingolipids at the molecular species level based on N-acyl chain composition. Total sphingolipid abundances were calculated by adding individual sphingolipid species for multivariate and univariate analyses across cell lines and infection conditions.

Sphingolipid profile differed across both cell types and during Sne infection. The major driver of lipid variation was cell origin (PERMANOVA, p = 0.001), followed by infection (PERMANOVA, p = 0.002). In addition, the magnitude of infection-associated sphingolipid remodeling differed between HeLa and HUVEC cells, as indicated by a significant interaction between cell line and infection status (PERMANOVA, p = 0.032) (Fig. 1a, **Supp.** Figure 1a).

Univariate analysis showed distinct cell type-associated but overlapping infection-associated changes in total sphingolipid classes. In HeLa cells, infection significantly reduced total dihydrosphingosine (dhSph, p = 0.002), sphingosine (Sph, p = 0.0001), SM (p = 0.0001) and glycosphingolipids, hexosylceramide (HexCer, p = 0.007) and lactosylceramide (LacCer, p = 0.019), while increasing S1P (p = 0.019) and dihydroceramide (dhCer, p = 0.00295). In HUVECs, infection led to significant decreases in dhSph (p = 0.0029), Sph (p = 0.002), S1P (p = 0.007), and SM (p = 0.002) (Fig. 1b). Analysis of individual sphingolipid species revealed similar patterns in these two cell types. Notably, the amounts of long-chain species of dhCer were increased in infected HeLa cells (**Supp.** Figure 1b).

To further assess the changes, we analyzed ratios between key lipid classes. Interestingly, we observed similar trends in both HeLa and HUVEC cells, with a reduction of the SM/Cer ratio, and an increase in the Cer/Sph and S1P/Sph ratios, indicating enhanced Cer breakdown and increased downstream Sph metabolism **(**Fig. 1c, d**)**.

Together, these findings demonstrate that Sne infection induces a conserved remodeling of the Cer-Sph-S1P pathway in both epithelial and endothelial cells, marked by SM loss and diversion of Cer into downstream metabolites, and that the magnitude and species distribution of these changes are cell type dependent.

Pharmacological inhibition of host sphingolipid pathways reveals pathway-specific effect on Simkania negevensis infection

To investigate the metabolic origin of the infection-associated sphingolipid remodeling, we treated HeLa cells with inhibitors of sphingolipid metabolism pathways and monitored the effect on Sne infection. Specific enzymes, from *de novo* sphingolipid synthesis, over lysosomal salvage of sphingolipids to inter-organelle transport, were targeted. Cells were pre-treated with two inhibitors of ASM, ARC39, which acts as an ASM active-site blocker [28], and desipramine, a lysosomotropic molecule belonging to functional inhibitors of ASM (FIASMA) that promotes ASM and AC degradation [29]. In addition, we used fluoxetine, which is a FIASMA that leads to degradation of not only AC, but also ASM, and AKS466, a fluoxetine

derivative with an increased AC specificity [30], to interfere with the salvage pathway. HPA-12, a CERT inhibitor [31], was used to target non-vesicular ER to Golgi Cer transport, and myriocin, a serine palmitoyltransferase (SPT) inhibitor [32], was used to suppress *de novo* sphingolipid synthesis in ER (**Supp.** Figure 2).

We quantified infection rates at 3 days p.i. by calculating the percentage of Sne-positive cells, as detected by the staining of bacteria with SnGroEL antibodies (Fig. 2, **Supp.** Figure 3). In a separate set of experiments, cells were not pretreated, but inhibitors were added only after Sne infection had already been established (at 6 h p.i.) (**Supp.** Figure 4).

Both treatment with ARC39 and desipramine led to a significant, dose-dependent reduction in the number of infected cells (Fig. 2a, b, **Supp.** Figure 3a, b). This effect was present even when the inhibitors were added later in infection, indicating that the inhibition of ASM does not influence the uptake of Sne but affects the development of the SnCV (**Supp.** Figure 4a, b). CERT inhibitor HPA-12, however, showed effect only when the cells were pretreated (Fig. 2c, **Supp.** Figure 3c), but not when infection had been already established (**Supp.** Figure 4c). Interestingly, inhibition of *de novo* Cer synthesis in the ER by myriocin had no influence on the number of Sne-infected cells in either experimental setup (Fig. 2d, **Supp.** Figure 3d, **Supp.** Figure 4d). Finally, we observed a reduction in infection rate upon treatment of cells with AC inhibitors fluoxetine and AKS466 (Fig. 2e, **Supp.** Figure 4e), which, in addition, showed a strong effect on the SnCV morphology (**Supp.** Figure 3e).

Hence, these data indicate that host SM turnover and Cer degradation to Sph in lysosomes limit Sne infection both at entry and during intracellular development, whereas inhibition of *de novo* sphingolipid synthesis has little impact, consistent with a reliance on the salvage pathway.

Inhibitors show distinct sphingolipid remodeling signatures in Simkania negevensis-infected epithelial cells.

To further investigate the alterations in sphingolipid profiles upon inhibitor treatment combined with infection in HeLa cells, we performed targeted quantification using tandem LC-MS/MS. Due to different solubilities, we grouped water-soluble and DMSO-soluble inhibitors separately for global lipidomic analysis (Fig. 3a, **Supp.** Figure 5a).

Multivariate analyses showed that inhibitors of sphingolipid biosynthesis reshape the total lipid profile in uninfected cells. Treatment with water-soluble inhibitors (ARC39, desipramine) demonstrated distinct variation in global sphingolipid profile, although there was no significant difference (PERMANOVA, $p = 0.151$), which is consistent with a moderate but heterogeneous impact of ASM pathway inhibition on basal sphingolipid composition. DMSO-soluble inhibitors (AKS466, HPA-12, and myriocin) also show clear segregation and significant difference in lipid profiles (PERMANOVA, $p = 0.028$) (Fig. 3a, **Supp.** Figure 5a).

In Sne-infected cells, global variations in total sphingolipid profiles were driven by both the inhibitors and infection status. Lipid profiles in cells treated with water-soluble inhibitors, ARC39 and desipramine, were significantly different (PERMANOVA, p = 0.002), which became even more apparent during infection (PERMANOVA, p = 0.001). Although DMSO-soluble inhibitors AKS466, HPA-12, and myriocin induced significant changes (PERMANOVA, p = 0.001), infected samples did not display significant global changes in total sphingolipids (PERMANOVA, p = 0.107) (**Supp.** Figure 5a).

At the level of individual sphingolipid species, the pattern was similar but more pronounced. Water-soluble ASM inhibitors (ARC39 and desipramine) induced clear and significant segregation of lipid profiles according to both inhibitor treatment (PERMANOVA p = 0.001) and infection status (PERMANOVA p = 0.001). Similarly, DMSO-soluble inhibitors (AKS466, HPA-12, and myriocin) produced distinct lipidomic separation primarily driven by inhibitor treatment (PERMANOVA p = 0.001), whereas infection contributed in a minor, non-significant way (p = 0.152) (**Supp.** Figure 6a).

Together, these analyses demonstrate inhibitor-specific sphingolipid signatures on both class and species levels, and that inhibitor identity, not infection status, is the predominant determinant of the global sphingolipid landscape under our experimental conditions.

Next, to investigate the contribution of each sphingolipid class during pathway inhibition and infection, we performed univariate analyses (Fig. 3b-f). ASM inhibitors ARC39 and desipramine both altered lipid abundances in uninfected cells (Fig. 3b, c). Interestingly, treatment with these inhibitors did not lead to the expected increase in SM levels typically associated with ASM inhibition. Instead, ARC39 significantly increased the amounts of HexCer (p = 0.0026) and LacCer (p = 0.0266) (Fig. 3b, **Supp.** Figure 5b), whereas desipramine treatment showed a similar but non-significant trend (Fig. 3c, **Supp.** Figure 5c). However, in infected cells, ARC39 treatment, in addition to increasing glycosphingolipids, significantly increased the abundances of dhSph (p = 0.0187), dhCer (p = 0.0002) and dhSM (p = 0.0039), whereas it decreased S1P (p = 0.00002) levels (Fig. 3b, **Supp.** Figure 5b). Desipramine treatment also significantly increased dhSph (p = 0.0384), dhCer (p = 0.0218), total Cer (p = 0.0459), and dhSM (p = 0.0271), while S1P (p = 0.0286) was significantly reduced (Fig. 3c, **Supp.** Figure 5c), implying infection-dependent enhancement of *de novo* sphingolipid synthesis when lysosomal ASM and the salvage pathway are inhibited.

Univariate analysis of individual sphingolipid species in ARC39 and desipramine-treated infected and non-infected cells was comparable to that of total sphingolipid classes. The increase in dhCer and dhSM was comparable across all chain lengths, although it was significant mostly for long chain species (**Supp.** Figure 6b, c).

These data indicate that ASM inhibition is associated with infection-dependent remodeling of sphingolipid metabolism. Interfering with cellular ASM activity promoted glycosphingolipid accumulation without major changes in total cellular SM, indicating altered SM turnover instead of classical bulk SM storage. Infection induced the accumulation of Cer precursors within the *de novo* synthesis pathway and

further increased the flux to dhSM synthesis. Desipramine treatment additionally elevated total Cer levels, consistent with its reported inhibitory effects on acid ceramidase activity [33].

Next, we targeted the *de novo* sphingolipid synthesis pathway by inhibiting SPT, the first committed enzyme, with myriocin, which significantly reduced total Cer ($p = 0.0112$) in uninfected cells, with a marginal but non-significant decrease in dhCer, among others. In infected cells, no sphingolipid class was significantly changed, although the amounts of all sphingolipids showed a downward trend, except S1P, which was increased (Fig. 3d, **Supp.** Figure 5d). At the level of individual sphingolipid species, the effect of myriocin was likewise more apparent in uninfected cells, with a significant reduction in all Cer species except Cer 20:0 and HexCer 24:1 ($p = 0.0382$). In infected cells, only Cer 16:0 ($p = 0.0290$) was significantly reduced, indicating that Cer loss could be compensated for by other pathways (**Supp. Figure 7a**). Considering that myriocin treatment did not affect infection, this suggests that *de novo* sphingolipid synthesis does not contribute to infection-associated sphingolipid remodeling.

Upon inhibition of CERT-dependent Cer transport from ER-to-Golgi by HPA-12, only dhSM ($p = 0.0150$) and SM ($p = 0.0495$) amounts were significantly reduced, with a modest but non-significant decrease in dhCer and an increase in glycosylated Cer. In infected cells, an additional significant reduction in dhCer ($p = 0.0314$) was observed, whereas total SM showed a non-significant decrease (Fig. 3e, **Supp.** Figure 5e). At the level of individual sphingolipid species, HPA-12 significantly reduced dhCer 16:0 in uninfected ($p = 0.0298$) and infected cells ($p = 0.00906$), and further reduced dhCer 24:0 ($p = 0.0236$) and dhCer 24:1 ($p = 0.0483$) in infected cells. A strong and consistent reduction was also seen across dhSM species regardless of infection, with non-infected cells additionally demonstrating significant reduction in multiple SM species (**Supp. Figure 7b**). As expected, CERT-dependent ceramide transport is required to maintain SM levels, of which a large part occurs in the Golgi. Interestingly, the increase in glycosylated Cer species, which are also produced in the Golgi [34], indicates an important contribution of other, CERT-independent, routes of Cer transport to its distribution within the cell. Sne infection additionally perturbs the dhCer flux, whereas the remaining sphingolipid profile resembles the pattern seen under myriocin treatment, with a notable, though statistically non-significant, increase in S1P.

Finally, we used AKS466, a potential inhibitor of AC, which is an enzyme that degrades Cer into Sph and free fatty acids in lysosomes. In uninfected cells, AKS466 treatment led to a significant reduction in Sph ($p = 0.00463$), as expected. However, total Cer, SM, and HexCer levels were also reduced, while total dhCer ($p = 0.0363$) accumulated (Fig. 3f, **Supp.** Figure 5f). At the level of individual sphingolipid species, dhCer 18:0, 22:0, and 24:0 were significantly increased regardless of infection, with overall elevated levels of dhCer in infected cells, which is consistent with the upregulation of *de novo* synthesis. dhSM 20:0 was significantly increased in both conditions. Additionally, HexCer levels were generally reduced, with significant decreases in HexCer 16:0 and 24:1 in uninfected and HexCer 16:0 in infected cells. In contrast, LacCer 16:0 was significantly reduced only in non-infected cells (**Supp. Figure 8**).

The increase in dhCer, which is converted to Cer through the activity of dihydroceramide desaturase (DES) [35] was unexpected, so we next tested whether AKS466 directly inhibits DES. We performed an *in*

vitro DES activity assay in the presence of AKS466, quantifying the conversion of deuterium isotope-labeled substrate (d_7-dhCer 13:0) using LC-MS/MS. Remarkably, AKS466 reduced substrate conversion efficiency by more than 50% ($p < 0.0001$), suggesting that it might directly inhibit DES through a previously unknown mechanism (Fig. 3g). Together with the strong effect that AKS466 has on inclusion development, these results verify the importance of the salvage pathway and DES activity as the potential Cer and SM source in Sne infection.

Genetically modified cells support Simkania negevensis dependence on SM/Cer turnover.

To avoid reliance on inhibitors, we turned to genetically modified cell lines, with ASM knockdown (kd), AC knockout (ko), and CERT ko [36], and compared the infection rate with the parental wild type (WT) HeLa cells. Ten ASM kd clones were tested for ASM activity (**Supp. Figure 9a**), and we selected two clones that showed a reduction in ASM activity similar to the treatment with ASM inhibitors ARC39 or amitriptyline (**Supp. Figure 9b, c**). The deletion of AC was confirmed by qPCR and compared to the siRNA-mediated knockdown, with one clone selected for further experiments (**Supp. Figure 9d**). Since fetal calf serum (FCS) used as a supplement for cell culture medium contains sphingolipids that can be taken up by the cells to compensate for the deficit [37], we performed the experiment under serum-reduced conditions (10%, 5%, and 2.5% FCS). With standard 10% FCS, infection rates were similar across all genotypes. However, in ASM kd and AC ko cells, infection rates significantly dropped to ~ 60–70% (Fig. 4a) and ~ 45% (Fig. 4c) when cells were grown with 5% and 2.5% FCS. In contrast, infection rates in CERT ko cells remained comparable to WT across all tested conditions (Fig. 4b). Together, these findings indicate that the salvage pathway, but not CERT-dependent ceramide transport, becomes critical for Sne infection when exogenous lipid supply is limited, which can mask pathway-specific requirements.

Simkania negevensis infection requires continuous SMS-driven Cer/SM flux, but is not affected by a transient depletion of plasma membrane SM.

Considering that we consistently observed that Sne infection significantly reduces SM levels (Fig. 1b, **Supp.** Figure 1b), we next aimed to investigate the role of SM synthesis in this process. For this, we quantified Sne infection rate in WT and stable SMS 1/2 double knockout (dko) HeLa cells. For analyzing the role of individual SMS enzymes, we created an anhydrotetracycline (AHT)-inducible complementation cell lines expressing wild-type SMS1 ($SMS1^C$ WT) or SMS2 ($SMS2^C$ WT), as well as $SMS2^C$ M64A and $SMS2^C$ M64R variants, which are catalytically active but mislocalized to the ER [38, 39]. The loss of SMS activity in SMS 1/2 dko, and its restoration in $SMS1^C$ WT upon AHT induction was confirmed by the FRET assay (**Supp. Figure 9e**) [40]. Sne infection rate was significantly reduced in SMS 1/2 dko cells, indicating that the absence of host cell SMS activity strongly impairs infection (Fig. 5a). AHT treatment alone did not significantly alter infection rates, but induction of SMS1 expression by AHT restored infection (Fig. 5b). Induction of SMS2 expression also led to the partial restoration of infection when compared to SMS1/2 dko. However, upon introduction of the SMS2 ER-mislocalized variants, Sne infection levels remained comparable to those of the dko mutant (Fig. 5a). This indicates that correct

localization of SMS2 to the plasma membrane is required for efficient infection, which is negatively affected by the perturbation in the ER lipid content.

To further explore if plasma membrane SM contributes to infection, we pretreated HeLa cells with *Staphylococcus aureus* β-toxin for 75 mins, which is known to hydrolyze plasma membrane SM and negatively affect *S. aureus* internalization [41]. Sne infection rates were unaltered upon treatment when compared to untreated cells. On the other hand, *S. aureus* showed a significant reduction in internalization under similar conditions, confirming the efficacy of plasma membrane SM depletion by β-toxin (Fig. 5c).

These results indicate that Sne relies on SM production mediated through the Cer-SM pathway and is sensitive to the changes in the ER lipid profile. Whereas plasma membrane SM is not required for Sne uptake, it might play a role in later stages of infection.

Targeted lipidomics reveals SM depletion and glycosphingolipid remodeling in SMS1/2 mutant cells

We next investigated the lipid profile of SMS1/2 dko, as well as complemented cell lines, with and without Sne infection. Global multivariate analysis across all samples showed that both SMS expression (genotype, MANOVA, $p < 0.0001$) and infection (MANOVA, $p < 0.0001$) significantly contributed toward sphingolipid variation. In addition, we observed significant interaction effects between genotype and infection (MANOVA, $p < 0.0001$), indicating genotype-dependent shifts in lipid profiles during infection (Fig. 6).

Principal component analysis showed that in the absence of infection, total and individual sphingolipid profiles originating from the loss of SMS activity (SMS1/2 dko and non-induced complementation cell lines, i.e., -AHT) clustered together, whereas WT and induced complementation cells displayed similar profiles consistent with restoration of sphingolipid homeostasis. However, during infection, induction of SMS1 expression still displayed a lipid profile similar to that of SMS1/2 dko. In addition, ER mislocalized $SMS2^{C}$ M64R demonstrated a sphingolipid signature distinct from WT or SMS1/2 dko (Fig. 6a, **Supp. Figure 11a**). The significant interaction between genotype and infection indicated that infection-associated sphingolipid remodeling is not uniform across all SMS genotypes.

Univariate analysis of total sphingolipids showed that, regardless of infection, SMS1/2 deletion led to a reduction of dhSM ($P < 0.0001$) and SM ($P < 0.0001$) and accumulation of HexCer ($P < 0.0001$) and LacCer ($P < 0.0001$) together with elevated S1P ($P < 0.0001$) when compared to the WT (Fig. 6b, c, **Supp. Figure 10**). Thus, in the absence of SMS1 or SMS2, sphingolipid flux is redirected away from SM toward glycosphingolipid and Sph/S1P pools.

Within the SMS1-complementation cell lines, $SMS1^{C}$ WT (-AHT) closely resembled the SMS1/2 dko sphingolipid profile, whereas AHT induction of $SMS1^{C}$ WT expression shifted the sphingolipid profile to

that of the WT. However, the abundances of dhSph, Sph, and S1P, as well as HexCer and LacCer, were still high, indicating an incomplete restoration of SM homeostasis. SMS2^{C} WT cell line followed a similar overall direction, where non-induced cells resembled SMS1/2 dko, while induction of SMS2 expression increased dhSM, SM, and dhCer and decreased glycosylated Cer and S1P. Sphingolipid profile of SMS2^{C} M64R was partly comparable to that of SMS2^{C} WT, except for elevated levels of dhSph, Sph, dhCer, and Cer, indicating an increase in *de novo* Cer synthesis (Fig. 6b, c, **Supp. Figure 10**). Thus, expression of SMS2 produced an intermediate sphingolipid profile instead of WT-like, which depended on the SMS2 localization and showed partial restoration of SM and dhSM levels and increased glycosylated Cer.

Analysis of individual sphingolipid species demonstrated a similar pattern to that of total sphingolipids. SMS1 and SMS2 expression uniformly restored dhSM and SM levels across all chain lengths. SMS2 expression additionally led to an increase in dhCer and Cer. Expression of SMS2 M64R showed a characteristic sphingolipid pattern with elevated dhSph, Sph, dhCer, Cer, dhSM, and SM, with a preference for short-chain sphingolipids (**Supp. Figure 11b, Supp. Figure 12**).

In infected cells, a similar pattern was observed, but with the more pronounced sphingolipid remodeling. This included an SM-rich, glycosphingolipid-poor pattern in infected SMS1/2 WT cells and high glycosylated Cer and low SM levels in infected SMS1/2 dko cells. Both non-induced SMS1^{C} WT and non-induced SMS2^{C} WT still showed SMS1/2 dko-like sphingolipid profiles when. Upon reconstitution of SMS2 or SMS2 M64R, the levels of total dhSM and SM were restored, whereas the reduction in S1P was still observable. However, the increase in dhCer and Cer in SMS2^{C} WT AHT-induced cells was absent upon infection, while dhCer and Cer levels were reduced, in contrast to the previous observation. Furthermore, infected SMS2^{C} M64R-expressing cells showed a characteristic lipid profile, similar to that of non-infected cells. However, the most striking difference was observed in infected cells with restored SMS1 expression. Instead of the expected increase in dhSM and SM, these sphingolipids remained low, while HexCer and LacCer remained comparatively high, suggesting that SMS1 expression could not restore SM production when cells were infected with Sne (Fig. 6b, c, **Supp. Figure 10, Supp. Figure 13**).

At the individual sphingolipid species level, overall lipid mirrored total sphingolipid level changes and showed that remodeling affected broad groups of sphingolipids. In uninfected SMS1/2 WT and DKO cells, multiple dhSM and SM species (dhSM 16:0/24:1, SM 16:0/24:1) were coordinately depleted, while corresponding HexCer and LacCer species were strongly enriched. Non-induced WT SMS1 or SMS2 cell lines reproduced the SMS1/2 dko pattern. SMS2- and SMS2 M64R-expressing cells showed restored SM species even upon infection, although HexCer and LacCer remained elevated compared to WT. On the contrary, cells expressing SMS1 showed no increase in dhSM or SM during infection (**Supp. Figure 11b, Supp. Figure 12**).

Together, these analyses show that loss or incomplete restoration of SMS activity shifts the sphingolipid profile away from SM toward glycosphingolipids. This effect becomes more evident during infection. Interestingly, in cells complemented for SMS1 expression, dhSM and SM remain reduced, indicating that

Sne infection particularly influences Golgi-localized SM biosynthesis and depends on continuous, properly localized SMS-driven sphingomyelin homeostasis.

Discussion

Sphingolipids are constitutive elements of membranes, as well as components of signaling pathways with an important role in immune response, cell death, and cell survival. For obligate intracellular bacteria, such as Sne, sphingolipids play a dual role as they are acquired by bacteria for replication, while sphingolipid-mediated immune response and cell death pathways must be inhibited by the pathogen [16, 42].

Our study focuses on understanding how Sne infection affects, as well as depends on, the sphingolipid metabolism of the host cell. Our results show that Sne infection leads to a reduction in SM, Cer, and Sph amounts, whereas S1P levels increase (Fig. 1). The differences observed for HeLa and HUVECs could be the consequence of different cell types (epithelial vs. endothelial) or different growth media and infection times (3 days vs. 2 days, due to the faster development of SnCV in HUVECs). However, the SM/Cer and Cer/Sph ratios show a similar trend in both cell types (Fig. 1c, d). HUVECs have high levels of S1P already without infection, which is known to regulate endothelial cell integrity and barrier function [43]. It is therefore possible that epithelial HeLa cells react to infection by S1P increase to mount an immune response, whereas HUVECs react in an opposite manner, which results in the increased permeability of an endothelial barrier, reflecting the events that happen *in vivo* during infection. Our subsequent experiments were performed using HeLa cells, because epithelium is the most likely site of first contact with Sne, and due to the availability of genetically modified cell lines.

S1P is a signaling molecule that modulates cellular immune response and acts as a pro-survival signal [44], and is often involved in bacterial and viral infections [45, 46]. We did not observe S1P increase only when ASM and AC were inhibited (Fig. 3). This indicates that the origin of S1P is downstream from ASM and AC, possibly through increased activity of the sphingosine kinase (SphK), which has been observed in infections involving viruses [46] and some bacteria [47, 48], either as a part of cellular immune response, or to serve as a pro-survival signal [49]. Another alternative is that a potential bacterial SphK, which has been identified in the Sne genome (SNE_A07170) [50] might also contribute to the S1P increase in infected cells.

We additionally detected a consistent increase in the levels of dhCer upon infection, which was especially pronounced in the cells treated with the ASM and AC inhibitors, where dhSM was also increased (Fig. 1, 3). dhCer and dhSM increases could be a response to infection, since higher amounts of dihydrosphingolipids enhance the rigidity of the cell membrane, which impairs viral infection [51]. Likewise, *Neisseria meningitidis* increases dhCer levels through the inhibition of the DES activity (Alina Weinmann, personal communication, and https://www.sphingolipidbiology.com/speakers/alina-weinmann). Therefore, the suppression of DES activity in infected cells and an increase in dhCer and dhSM could be a part of the cellular immune response to infection.

The observed dhCer increase was not present when the *de novo* synthesis or Cer transport by CERT was inhibited (Fig. 1, 3). The inhibition of SPT by myriocin would inhibit the steps preceding dhCer synthesis, explaining this observation; however, CERT inhibition by HPA-12 did not lead to Cer accumulation as could be expected, but to a reduction in the levels of Cer and dhCer as well as dhSM and SM, and an increase in HexCer and LacCer (Fig. 3e, **Supp.** Figure 5e). This reduction of dhCer after HPA-12 treatment has not been previously reported, though a reduction in SM and an increase in glycosylated Cer have [31], indicating either that this glycosylation could take place outside of the Golgi or that other, alternative ways of Cer transport to the Golgi exist.

Although HPA-12 inhibition of CERT transport diminished the infection rate in a dose-dependent manner (Fig. 2c), we could not reproduce this effect with a CERT ko cell line (Fig. 4b), and the inhibitor had no effect when added at the later stages of infection (**Supp.** Figure 4c). This is in contrast with the role of CERT in the development of related bacteria, such as Ctr [23] and *C. psittaci* (Cps) [36]. CERT ko resulted in fewer infected cells and a smaller inclusion size [36] and induced premature egress of Cps from infected cells [52]. Sne, therefore, is exceptional in this regard. The recruitment of CERT to Sne is difficult to study, due to the morphology of inclusion, which is tubular, convoluted, and lined with the ER [13]. The proximity to the ER might circumvent the need for CERT because it facilitates lipid exchange. This is supported by our results, which show that the inhibition of CERT by HPA-12 at the later stages of infection and CERT ko did not have any effect on the number of infected cells or the SnCV itself (**Supp.** Figure 3c, **Supp.** Figure 4c, Fig. 4b). The fact that HPA-12 decreased Sne infection when added before infection points to a possible mechanism independent of CERT inhibition. HPA-12 is a Cer analog [31], so an off-target effect on other ceramide-binding proteins, maybe even of bacterial origin [53], or an anti-bacterial activity in general [54], cannot be excluded, though this is relevant only in the early stages of infection.

Another specificity of Sne is that, unlike Ctr, it is largely independent of the *de novo* Cer synthesis (Fig. 2d, **Supp.** Figure 3d, **Supp.** Figure 4d). SPT inhibition by myriocin or sphingosine N-acetyltransferase inhibition by fumonisin B1 affected Ctr inclusion development, morphology, and fusion, and led to premature release of EBs [55, 56]. In view of the Sne dependence on ASM and AC activity (Fig. 2a, b, e), it is conceivable that the bacteria derive most of their sphingolipids from the salvage pathway, possibly through Sph conversion to Cer in the ER, which can compensate for *de novo* pathway inhibition. The decrease of Sph in infected cells could in part reflect this fact (Fig. 1b-d). Further on, whereas AKS466 seems to have a broader influence on sphingolipid synthesis, inhibiting not only AC but also DES (Fig. 3g), the experiment with a cell line lacking AC confirmed Sne infection depends on AC (Fig. 4c). This would support bacterial dependence on the salvage pathway, as well as downstream metabolites such as Sph, to supply the growing inclusion with sphingolipids. The already reported role of retrograde transport in SnCV development [15], as well as the importance of late endocytic multivesicular bodies for Ctr infection [57], agree with our findings. Interestingly, blocking both the salvage pathway as well as *de novo* synthesis by AKS466 had the most pronounced effect on the SnCV (**Supp.** Figure 3e). Bacteria, therefore, might be able to compensate for the inhibition of the salvage pathway by deriving metabolites from the *de novo* synthesis and cannot develop when both pathways are inhibited simultaneously.

Related organisms, such as Ctr and Cps, depend on SM for development and inclusion stability, and this is also true for Sne. Ctr has been shown to recruit SMS1/2 to inclusion together with CERT to form platforms for conversion of Cer into SM [23]. However, a later report demonstrated that Ctr infects and develops normally in SMS1/2 dko cells, even in the low-serum conditions. However, CERT deletion alone under low-serum conditions, as well as triple knockout of SMS1/2 and CERT, strongly reduced the Ctr infection rate [58]. This is the opposite of what we observe for Sne (Fig. 4b, Fig. 5a, b) and points to crucial differences between Sne and other *Chlamydia* in the way they obtain Cer and SM. Ctr can convert Cer into SM even in the absence of host cell enzymes SMS1/2 [58], implying the existence of a bacterial enzyme with SMS activity. Sne is not known to possess such an enzyme, though two putative sphingomyelinases have been identified in its genome (SNE_A21560 and SNE_A12690) [50]. Furthermore, Sne infection is sensitive to the source of the host cell SM and the localization of SMS. Expression of SMS2, which localizes to the plasma membrane, in SMS1/2 dko cells could partially recover Sne infection, and so could the expression of the Golgi-localized SMS1. When we expressed an SMS2 mutant enzyme that mislocalized to the ER, which is connected to various pathologies in humans [38], Sne infection rate remained low (Fig. 5a, b). This shows that bacteria can retrieve SM from the plasma membrane and Golgi, but that they are sensitive to the perturbation of the ER SM content, emphasizing the close relationship between SnCV and ER.

Sphingolipidome analysis of SMS1/2 dko showed the expected decrease in SM and already reported increase in glycosylated Cer once SM biosynthesis was abolished [58, 59]. This could be reverted successfully by the expression of either variant of SMS, though the expression of the pathogenic, mislocalized SMS2 M64R variant yielded a specific pattern, with an increase in metabolites upstream of SM synthesis, such as dhSph, dhCer, and Cer, possibly reflecting a perturbation in the *de novo* synthesis pathway (Fig. 6b). However, the expected increase in SM was completely absent in Sne-infected cells expressing only an SMS1 WT enzyme (Fig. 6b, c). Considering that the bacterial infection rate is restored in this setup, it is unlikely that Sne infection blocks SMS1 activity. One possibility would be that bacteria specifically metabolize Golgi-produced SM, perhaps through the activity of their own sphingomyelinases, leading to low SM levels and increased levels of HexCer and LacCer. Ctr is known to depend on the Golgi for lipid acquisition, leading to the Golgi fragmentation [24] or redirection of the sphingolipid vesicular transport from the Golgi to the Ctr inclusion [60]. We have not observed Golgi fragmentation in Sne infection, but our data also imply an important function of this organelle in the Sne life cycle.

In conclusion, we provide a detailed analysis of the role of host-cell sphingolipid metabolism in the life cycle of an obligate intracellular *Chlamydia*-like bacterium. We reveal unique aspects of the biology of this organism, which make it different from all other so far studied *Chlamydia*. Sne, characterized by host promiscuity and an unusually long life cycle, develops in a salvage pathway-dependent, CERT- and *de novo* synthesis-independent way. Bacteria rely on ASM and AC, utilizing Golgi-localized SMS1-produced SM pool, and are sensitive to perturbations of the ER sphingolipid content. Our data, coupled with the in-depth analysis of the sphingolipid profile of cells treated with different inhibitors of sphingolipid synthesis, offer a valuable source of information on the effect of inhibitors and infection on the metabolism of sphingolipids, and characterize for the first time the exceptional features of *Simkania*

negevensis sphingolipid acquisition, which contribute to the infectivity and adaptability of this fascinating bacterium.

Materials and methods

Cell culture

HeLa (ATCC CCL-2) and HeLa229 (ATCC CCL-2.1) cells were cultured in RPMI-1640 medium supplemented with GlutaMAX (Gibco, Cat. No. 72400021) and 10% (v/v) heat-inactivated (56°C at 30 min) fetal bovine serum (FBS; Sigma-Aldrich, Cat. No. F7524). For HeLa (CCL-2) cultures, the medium was further supplemented with 1 mM sodium pyruvate (Gibco, Cat. No. 11360088). Both HeLa cell lines were routinely tested for *Mycoplasma* contamination by polymerase chain reaction (PCR) and confirmed to be negative. As authentication had been performed by ATCC, no additional validation was carried out in our laboratory.

U2OS and Hek293T cells were maintained in DMEM high glucose medium (Sigma-Aldrich, Cat. No. D6429) supplemented with 10% (v/v) heat-inactivated FBS.

Human umbilical vein endothelial cells (HUVEC) (Gibco, Cat. No. C01510C) were cultured in VascuLife basal medium (CellSystems, Cat. No. LM-0002) complemented with microvascular growth supplement (CellSystems, Cat. No. LS-1020) and 5% (v/v) heat-inactivated FBS.

Cells were seeded either one day (HeLa and HeLa229) or two days (HUVEC) before the experiment. Standard tissue culture procedures were used to maintain the cells. All cells were cultured in a humidified atmosphere with 5% CO_2 (v/v) at 37°C.

Bacteria and infection

Simkania negevensis (ATCC VR-1471) was prepared according to a previously published protocol [61]. All experiments were performed under biosafety level 2 (BSL-2) conditions in a laboratory registered with the Government of Lower Franconia (registration code: 55.1-8791.1.30).

For infection experiments, cells were seeded into a 12-well plate (1 x 10^5 or 2 × 10^5 cells per well) or into a 6-well plate (5 × 10^5 cells per well). At approximately 60% confluency, cells were infected with Sne at a multiplicity of infection (MOI) of 1 in RPMI-1640 GlutaMAX Supplement (Gibco, Cat. No. 61870044) medium supplemented with 5% (v/v) heat-inactivated FBS (infection medium). Plates were centrifuged at 900 × g for 1 h at 35°C to synchronize infection, followed by incubation for 5 h at 35°C and 5% CO_2 in a humidified incubator. At 6 h p.i., the medium was aspirated and replaced with fresh infection medium. Infected cells were maintained under these conditions for 3 days.

For the infection under low serum conditions, each line was adapted for approximately one week to RPMI containing either 10% heat-inactivated FCS, 5% heat-inactivated FCS, or 2.5% non-inactivated FCS

to obtain sufficient cell numbers. Cells were then seeded and infected as described above.

Inhibitor treatment with infection

Infection studies in the presence of pharmacological inhibitors (ARC39 [28], desipramine [29], AKS466 [30], HPA-12 [31], and myriocin [32]) were performed using HeLa229 cells. Cells were seeded at a density of 1×10^5 cells per well onto 15-mm glass coverslips placed in 12-well plates and incubated overnight at 37°C in a humidified atmosphere containing 5% CO_2. The next day, cells were pre-incubated for 3 h with the respective inhibitors or controls (water or DMSO; Carl Roth, cat no. A994.2) in the infection medium. After pre-incubation, cells were infected as described above. Medium was replaced with fresh infection medium containing the corresponding inhibitor or control at 1- and 2-days p.i.

In a separate set of experiments (**Supp.** Figure 4), inhibitor treatment was initiated after the establishment of infection. HeLa cells were first infected as described above and incubated for 6 h. At 6 h p.i., the infection medium was replaced with infection medium containing the respective inhibitors or controls. Thereafter, medium exchange with fresh inhibitor- or control-containing infection medium was performed every 24 h for 3 days.

At 3 days p.i., cells from all experimental conditions were washed once with 1×DPBS (Gibco, Cat. No. 14190144), fixed with 4% paraformaldehyde (PFA), washed three times with 1×DPBS, and stored in 1×DPBS at 4°C until immunostaining.

Immunofluorescence staining and microscopy.

Cells were fixed with 4% (w/v) PFA for 30 min at room temperature, permeabilized with 0.2% (v/v) Triton X-100 (Carl Roth, cat no. 3051.4) in 1×DPBS for 15 min, and washed with 1×DPBS. The cells were blocked with 2% (v/v) goat serum (Gibco, Cat. No. 16210-064) in DPBS for 1 h at room temperature with gentle shaking. Samples were then incubated overnight at 4°C with rabbit anti-*Simkania* (SnGroEL, homemade against the full-length GroEL from *S. negevensis*, Gramsch Laboratories) [13] primary antibodies diluted 1:800 in 2% (v/v) goat serum. Following washing with 1×DPBS, coverslips were incubated for 1 h at room temperature using fluorophore-conjugated secondary antibodies, anti-rabbit AlexaFluor 488 (Thermo Fisher, Cat. No. A-11008) or AlexaFluor 555 (Thermo Fisher, Cat. No. A-21428) diluted 1:200 in 2% (v/v) goat serum, together with DAPI (Merck, Cat. No. D9542-5MG) (1:1000). Coverslips were mounted using Mowiol (Carl Roth, Cat. No. 0713.1).

For each condition, three random pictures per coverslip were taken using identical acquisition settings on a Leica DMi8 (DFC 7000 T) inverted fluorescence microscope. Images were acquired in separate channels corresponding to the respective fluorophores and merged using FIJI/ImageJ [62]. Infected and total cells were manually counted. The infection rate was calculated as the ratio of infected cells per image to the total number of cells per image. For each condition, three technical replicates were averaged and normalized to the non-treated control. Data from three independent biological replicates

were plotted and statistically analyzed using GraphPad Prism. Statistical significance was determined by one-way analysis of variance (ANOVA) followed by Dunnett's multiple comparisons test.

Generation of genetically modified cell lines

HeLa ASM knockdown cell lines were generated by lentiviral transduction using a small hairpin RNA (ASM1-1: 5' – ACACCTGTCAATAGCTTCC – 3'; ASM1-2: 5' – TGGAATTATTACCGAATTG – 3') targeting SMPD1, cloned into the pLVTHM vector as described previously [63]. Transduced cells were single-cell sorted using a FACSAria III (BD Biosciences) into 96-well plates. Ten independent clones were expanded and screened for ASM activity (**Supp. Figure 9**).

For AC knockout in HeLa cells, two AC (ASAH1)-specific gRNAs (5' – GGAACATAAATAATGATACC – 3' and 5' – TTCAAGCTTTGCTGGCTATG – 3') were cloned into the pSpCas9(BB)-2A-GFP vector (Addgene Plasmid #48138) by restriction digestion using Fast Digest BpiI (BbsI) (Thermo Fisher, Cat. No. FD1014). HeLa cells were then transfected with the 2 µg of plasmid using commercially available transfection reagent jetOPTIMUS (Polyplus, Cat. No. 101000051). After 24 h, GFP-positive single cells were sorted into 96-well plates using a FACS Aria III (BD Biosciences) and clonally expanded. The resulting clones were subsequently analyzed for AC expression by RT-qPCR.

CERT knockout HeLa cells and the corresponding wild-type control cell line were kindly provided by the laboratory of Dagmar Heuer and have been described previously [36].

SMS1/2 wild-type (WT), SMS1/2 double-knockout (dko), SMS2-complemented dko ($SMS2^{C}$ WT), and SMS2-M64R–expressing dko ($SMS2^{C}$ M64R) cell lines were generated in the laboratory of Joost Holthuis, as reported earlier [38].

Complementation of sphingomyelin synthase 1 (SMS1) was performed in SMS1/2 dko HeLa cells as previously described with modifications [38, 39]. Hek293T cells were co-transfected with a tetracycline-inducible lentiviral construct pInducer20-FLAG-SMS1 together with the packaging plasmids psPAX and pVSV-G using the Ca^{2+}-phosphate method [63]. The culture medium was changed 6 h post-transduction. After 48 h, the lentivirus particles were harvested and used to infect HeLa SMS1/2 DKO cells in the presence of 0.5 µg/mL polybrene (Sigma-Aldrich, Cat. Nr. H9268). After 24 h, the medium was replaced with DMEM containing 1 mg/mL G418 (Sigma-Aldrich, Cat. Nr. G8168) to select for transduced cells. Following antibiotic selection, functional validation of SMS1 complementation was performed using FRET-based assays and lipidomics analysis.

The used cell lines are summarized in the **Supp. Table 1**.

ASM activity assay

ASM activity measurements were based on a previously published protocol [64, 65]. A day prior to the experiment, 0.5 x 10^5 cells per well were seeded in a 24-well plate. One set of samples was treated with ASM inhibitors 10 µM ARC39 or 20 µM amitriptyline (Sigma-Aldrich, Cat. Nr. A8404-25G). Cells were washed thrice with 1xDPBS and lysed by adding 100 µL per well of ASM lysis buffer (250 mM NaOAc pH 5.0, 0.1% Nonidet P40 substitute (AppliChem, Cat. No. A1694,0250), 1.3 mM EDTA, 1xProtease Inhibitor Cocktail (Sigma-Aldrich, Cat. No. 11873580001)) for 15 min at 4°C. Subsequently, cells were scraped from the well, centrifuged (14,000xg/3 min/4°C) to remove cell debris and protein concentration in the cleared lysates was determined via bicinchoninic acid (BCA) assay using the Pierce BCA Protein Assay Kit (Thermo Fisher, Cat. No. 23227) following the manufacturer`s instructions.

Consecutively, a volume corresponding to 1 µg protein was incubated with 100 µL ASM assay buffer (200 mM NaOAc pH 5.0, 500 mM NaCl, 0.02% Nonidet P40 substitute) containing 0.58 µM BODIPY-FL-C12-sphingomyelin (Thermo Fisher, Cat. No. D7711) on a shaker for 4 h/37°C/300 rpm. To stop the reaction and extract the lipids, 250 µL 2:1 $CHCl_3$/MeOH was added to the samples and mixed by vortexing. Samples were centrifuged (13,000xg/3 min), and 100 µL of the lower organic phase was taken. Next, the solvent was evaporated in a SpeedVac concentrator (Eppendorf) for 20 min/45°C, the lipid pellet was resuspended in 10 µL 2:1 $CHCl_3$/MeOH, and spotted in 2 µL steps onto a silica plate (Macherey-Nagel/VWR, Cat. No. 552–1006). Thin-layer chromatography was conducted with 80:20 $CHCl_3$/MeOH, and plates were scanned in a Typhoon 9200 fluorescence scanner (Cytiva) with 561 nm excitation. Band intensities of ceramide (upper band) and sphingomyelin (lower band) were measured in Fiji [62]. ASM activity was calculated based on converted substrate, the assay time, and the amount of lysate used for the assay. If indicated, ASM activities were normalized to those of untreated WT cells. Controls included untreated cells, as well as the cells treated with 10 µM ARC39 for 22 h and 20 µM amitriptyline (Sigma-Aldrich, Cat. Nr. A8404-25G) for 75 min. In HeLa ASM knockdown clones 2 and 6, the lowest activity was detected, and hence, these clones were used for further investigations (**Supp. Figure 9b, c**).

RT-qPCR

AC knockout in HeLa cells was validated by RT-qPCR (**Supp. Figure 9d**). Total RNA was isolated using the RNeasy Mini Kit (Qiagen) with DNase treatment, and 1 µg RNA was reverse-transcribed using the RevertAid First Strand cDNA Synthesis Kit (Thermo Fisher). RT-qPCR was performed on a StepOnePlus Real-Time PCR System using GreenMasterMix (Genaxxon). All reactions were performed in triplicate. Ct values were converted to mean using StepOne software. Relative gene expression was calculated using the $2^{-\Delta\Delta Ct}$ method [66], with GAPDH as the endogenous control. siRNA control was prepared using ON-TARGETplus Human ASAH1 siRNA - SMARTpool (Horizon, Cat. Nr. L-005228-03-0005), transfected with DharmaFECT (Horizon, Cat. Nr. T-2001-01) according to manufacturer's instructions. Primer sequences were as follows: AC forward 5' – GGAGTTGCGTCGCCTTAGTC – 3', reverse 5' – CTGCAGTCCTCTGTCCACG – 3'; GAPDH forward 5' – TGTCAAGCTCATTTCCTGGTATGA – 3', reverse 5' – CTTACTCCTTGGAGGCCATGTAG – 3'.

FRET-based SMS activity assay

To assess SMS activity, HeLa cells (0.5×10^5) were seeded onto sterile glass coverslips in 24-well plates and incubated for 24 h. Cells were then treated with 2.5 µM α-NH_2-ω-N_3-C_6-Ceramide [30] and 200 µM propargyl-choline (Jena Bioscience, Cat. No. CLK-066) [67] for an additional 24 h, resulting in biosynthesis of trifunctional sphingomyelin (TFSM) [68]. After treatment, cells were washed with DPBS and fixed with 4% PFA and 0.2% glutaraldehyde (GA) in DPBS for 30 min at room temperature, followed by permeabilization with 0.2% Triton X-100 for 20 min at room temperature. For donor dye labeling, cells were incubated with 0.5 µM BODIPY-FL-DBCO (Jena Bioscience, Cat. No. CLK-040-05) in HBSS for 1 h at 37°C/170 rpm. After washing five times with DPBS, cells were stained with 5 µM AZDye 546 Azide (Jena Bioscience, Cat. No. CLK-1283-AZ) in click reaction buffer (50 µM $CuSO_4$, 2.5 mM sodium ascorbate, 250 µM Tris(3-hydroxypropyltriazolylmethyl) amine (THPTA) in PBS) for 1 h at 37°C/170 rpm. The samples were then mounted in Mowiol (24 g glycerol, 9.6 g Mowiol 4–88 (Carl Roth, Cat. No. 0713.2), 48 mL 0.2 M TRIS-HCl pH 8.5, 24 mL pure water). FRET efficiency was determined using FRET acceptor bleaching with the built-in FRET acceptor bleaching wizard on a Leica Stellaris 5 confocal microscope. One-way ANOVA and Tukey's multiple comparison test were used in GraphPad Prism for statistical analysis. The full development of this assay is described in a separate publication [40].

DES activity assay

HeLa cells were seeded at 2×10^5 cells per well in 12-well plates and cultured until ~ 90% confluency. Cells were pre-incubated for 1 h at 37°C with 15 µM AKS466 or DMSO (solvent control) in RPMI supplemented with 10% heat inactivated FBS. Subsequently, 1 µM of the stable isotope–labeled dihydroceramide desaturase (DES) substrate d_7-dhCer 13:0 (Avanti Polar Lipids, Alabaster, AL, USA) was added directly to the wells, and cells were incubated for an additional 4 h at 37°C. After incubation, the culture medium was removed, and the cells were washed with ice-cold PBS. Cells were harvested on ice by scraping in 500 µL ice-cold LC-MS grade methanol, transferred to tubes, and stored at -80°C until lipid extraction as described below for the determination of the cellular sphingolipidome. For the analysis, a 1290 Infinity II HPLC coupled with a 6465B (Ultivo) triple-quadrupole mass spectrometer (Agilent Technologies, Waldbronn, Germany) was used. Chromatographic conditions and settings of the MS/MS detector were as described previously [69]. Multiple reaction monitoring (MRM) was applied to monitor cellular DES activity. To this end, peak areas of the substrate d_7-dhCer 13:0 as well as the product d_7-Cer 13:0 were normalized to the internal standard Cer 17:0 and quantified via Cer 16:0 external calibration using MassHunter Quantitative Analysis software (version 10.1, Agilent Technologies). Intracellular DES activity was determined as conversion rate (%) = c (d_7-Cer 13:0)/(c (d_7-dhCer 13:0) + c (d_7-Cer 13:0)) with c being the concentration (in nM) in the lipid extract.

β-toxin treatment

HeLa cells (2×10^5 cells/well; 12-well plates containing coverslips) were seeded 24 h prior to treatment. To deplete host sphingomyelin, cells were pretreated with *Staphylococcus aureus* β-toxin (Sigma-Aldrich, Cat. No. S8633-25UN) at 100 ng/mL for 75 min at 37°C; control wells received infection medium only.

Without removing the β-toxin-containing medium, cells were infected with *S. negevensis* as described above. At 6 h post-infection, the medium was exchanged with infection medium containing β-toxin (100 ng/mL), and infection was continued for 3 days with daily medium exchange, maintaining β-toxin. Cells were fixed with 4% PFA and immunostained for SnGroEL for fluorescence microscopy. β-toxin-pretreated *S. aureus* JE2 infection was performed in parallel as a positive control to verify β-toxin activity [41][13].

Quantification of sphingolipids by liquid chromatography tandem-mass spectrometry (LC-MS/MS)

For lipidomic analyses, 2×10^5 cells were seeded per well in 6-well plates under either inhibitor-treated conditions or using SMS1/2-modified cell lines. Cells were preincubated for 3 h with the indicated inhibitors or corresponding controls. Subsequently, cells were infected for 3 days at an MOI of 1, as described previously. For harvesting, cells were washed once with ice-cold 1×DPBS, detached by scraping, and resuspended in 500 µL of ice-cold methanol. Samples were stored at − 80°C until further processing.

Sphingolipids were extracted with 1.5 mL methanol/chloroform (2:1, v:v) containing the internal standards d_7-sphingosine (d_7-Sph), d_7-dihydrosphingosine (d_7-dhSph), d_7-sphingosine 1-phosphate (d_7-S1P), 17:0 ceramide (d18:1/17:0), d_{31}-16:0 sphingomyelin (d18:1/16:0-d_{31}), 17:0 glucosyl(β) ceramide (d18:1/17:0; 17:0 HexCer) and 17:0 lactosyl(β) ceramide (d18:1/17:0; 17:0 LacCer) (Avanti Polar Lipids, Alabaster, AL, USA). Extraction was facilitated by incubation at 48°C with gentle shaking (120 rpm) overnight. To reduce interference from glycerolipids, samples were saponified with 150 µL 1 M methanolic KOH for 2 h at 37°C with gentle shaking (120 rpm) followed by neutralization with 12 µL glacial acetic acid. After centrifugation at 2,200xg for 10 min at 4°C, organic supernatants were evaporated to dryness using a Savant SpeedVac concentrator (Thermo Fisher). Dried residues were reconstituted in 200 µL acetonitrile/methanol/water (47.5:47.5:5 (v:v:v), 0.1% formic acid) and subjected to LC-MS/MS sphingolipid quantification applying the multiple reaction monitoring (MRM) approach. Chromatographic separation was achieved on a 1290 Infinity II HPLC (Agilent Technologies, Waldbronn, Germany) equipped with a Poroshell 120 EC-C8 column (3.0 x 150 mm, 2.7 µm; Agilent Technologies) guarded by a pre-column (3.0 x 5 mm, 2.7 µm) of identical material. MS/MS analyses were carried out using a 6495C triple-quadrupole mass spectrometer (Agilent Technologies) operating in the positive electrospray ionization mode (ESI+). Chromatographic conditions and settings of the ESI source and MS/MS detector have been published elsewhere [69]. The mass transitions used for analysis of sphingolipid subspecies are given in **Supp. Table 2**. Peak areas of Cer, dhCer, SM, dhSM, HexCer and LacCer subspecies, as determined with MassHunter Quantitative Analysis software (version 10.1, Agilent Technologies), were normalized to those of their internal standards, followed by quantification via external calibration. Sph, dihydrosphingosine dhSph, and S1P were directly quantified via their deuterated internal standards.

Lipidomics data processing and statistical analysis

Lipidomics data were analyzed using the R statistical environment with custom analysis scripts (see Supp. Information for more details). Raw LC-MS/MS lipid abundance tables were combined with sample information, and lipids detected only at very low levels or in very few samples were removed. Data were $\log_{10}(x + 1)$ transformed, and missing values were handled conservatively without general imputation [70]. Depending on the analysis, lipid values were optionally scaled. Overall patterns in lipid profiles were explored using principal component analysis (PCA) and distance-based methods, while differences between experimental groups were tested using MANOVA or, when assumptions were not met, PERMANOVA with permutation testing. Individual lipid changes were analyzed using linear models with infection and treatment as factors, and relevant contrasts were extracted to compare conditions. Multiple testing was controlled using false discovery rate (FDR) correction. All plots were generated in R-Studio from the processed data.

Data and code availability

All supplementary data, including an overview of multivariate analyses, multiple comparison tables including False Discovery Rates, original microscopic and chromatography images, and raw data tables, are available as source data provided with this paper and at Zenodo (https://doi.org/10.5281/zenodo.18866967). The complete lipidomics analysis pipeline code, including all R markdown workflows and supporting scripts used for data preprocessing, statistical modeling, and figure generation, is publicly available on https://github.com/sudu87/human-cell-targeted-lipidomics-pipeline. Detailed information on all R packages, functions, and analysis parameters used is fully documented within the repository.

Declarations

Acknowledgments:

We would like to thank Sebastian Banhart and Dagmar Heuer from the Unit of Sexually Transmitted Bacterial Pathogens and HIV at the Robert Koch Institute for generously providing the CERT knockout cell lines used in this study. We thank Kerstin Paprotka for generating the ASM knockdown HeLa cell lines, Elke Maier, Kristyna Pekarkova, and Leonie Speth for their excellent technical assistance, Daniel Herrmann for the technical support during the LC-MS/MS analyses, and Fabienne Wagner and Mac Dang Giang for experimental support and helpful discussion.

Funding:

This work was supported by the Deutsche Forschungsgemeinschaft (DFG) within the research training group RTG2581 (M.F., B.K., J.S., V.K.P.). We would like to acknowledge the assistance of the Core Facility BioSupraMol supported by the DFG.

Contributions:

Conceptualization of this study: A.M, J.D.W., B.K., V.K.P.

Biological experiments & data analysis: A.M., J.D.W, F.Schu., M.R., S.S., H.S., F.Schm., S.D.

Data Curation: A.M., J.D.W., F.Schu., S.D., V.K.P.

Manuscript draft: A.M., J.D.W., S.D., V.K.P.

Chemical synthesis: D.B., J.S., C.K., C.A.

Resources: V.K.P., M.F., M.S., B.K.P., J.S., C.A., J.C.M.H.

Supervision & review: V.K.P., M.F., J.S., B.K., C.A., J.C.M.H., S.D., M.S.

All authors contributed to the article and approved the submitted version.

Ethics declaration:

The authors declare no competing interests.

References

1. Kahane S et al (1993) Description and partial characterization of a new chlamydia-like microorganism. FEMS Microbiol Lett 109(2–3):329–333
2. Donati M et al (2015) Prevalence of Simkania negevensis in chlorinated water from spa swimming pools and domestic supplies. J Appl Microbiol 118(4):1076–1082
3. Kahane S et al (2004) Evidence for the presence of Simkania negevensis in drinking water and in reclaimed wastewater in Israel. Appl Environ Microbiol 70(6):3346–3351
4. Kahane S et al (2001) Infection of Acanthamoeba polyphaga with Simkania negevensis and S. negevensis survival within amoebal cysts. Appl Environ Microbiol 67(10):4789–4795
5. Vouga M, Baud D, Greub G (2017) Simkania negevensis may produce long-lasting infections in human pneumocytes and endometrial cells. Pathog Dis, 75(1)
6. Lieberman D et al (1997) Pneumonia with serological evidence of acute infection with the Chlamydia-like microorganism Z. Am J Respir Crit Care Med 156(2 Pt 1):578–582
7. Vouga M, Baud D, Greub G (2017) Simkania negevensis, an insight into the biology and clinical importance of a novel member of the Chlamydiales order. Crit Rev Microbiol 43(1):62–80
8. Scaioli E et al (2019) Simkania negevensis in Crohn's Disease. Dig Dis Sci 64(11):3284–3290
9. Husain S et al (2007) Simkania negevensis in bronchoalveolar lavage of lung transplant recipients: a possible association with acute rejection. Transplantation 83(2):138–143
10. Greenberg D et al (2003) High rate of Simkania negevensis among Canadian inuit infants hospitalized with lower respiratory tract infections. Scand J Infect Dis 35(8):506–508
11. Kahane S, Kimmel N, Friedman MG (2002) The growth cycle of Simkania negevensis. Microbiology 148(3):735–742

12. Kahane S et al (1999) Simkania negevensis strain ZT: growth, antigenic and genome characteristics. Int J Syst Evol MicroBiol 49(2):815–820
13. Mehlitz A et al (2014) The chlamydial organism Simkania negevensis forms ER vacuole contact sites and inhibits ER-stress. Cell Microbiol 16(8):1224–1243
14. Koch R-D et al (2020) Modulation of Host Cell Death and Lysis Are Required for the Release of Simkania negevensis. Front Cell Infect Microbiol 10:594932
15. Herweg J-A et al (2016) Proteomic analysis of the Simkania- containing vacuole: the central role of retrograde transport: Simkania, proteomic and lipid trafficking. Mol Microbiol 99(1):151–171
16. Kunz TC, Kozjak-Pavlovic V (2019) Diverse Facets of Sphingolipid Involvement in Bacterial Infections. Front Cell Dev Biology 7:203
17. Simons K, Ikonen E (1997) Functional rafts in cell membranes. Nature 387(6633):569–572
18. Harvald EB, Olsen ASB, Færgeman NJ (2015) Autophagy in the light of sphingolipid metabolism. Apoptosis 20(5):658–670
19. Cuvillier O et al (1996) Suppression of ceramide-mediated programmed cell death by sphingosine-1-phosphate. Nature 381(6585):800–803
20. Gault CR, Obeid LM, Hannun YA (2010) An Overview of Sphingolipid Metabolism: From Synthesis to Breakdown. Sphingolipids as Signaling and Regulatory Molecules. Springer, New York: New York, NY, pp 1–23. C. Chalfant and M.D. Poeta, Editors
21. Hanada K et al (2003) Molecular machinery for non-vesicular trafficking of ceramide. Nature 426(6968):803–809
22. Huitema K et al (2004) Identification of a family of animal sphingomyelin synthases. Embo j 23(1):33–44
23. Elwell CA et al (2011) Chlamydia trachomatis Co-opts GBF1 and CERT to Acquire Host Sphingomyelin for Distinct Roles during Intracellular Development. PLoS Pathog 7(9):e1002198
24. Heuer D et al (2009) Chlamydia causes fragmentation of the Golgi compartment to ensure reproduction. Nature 457(7230):731–735
25. Rockey DD, Fischer ER, Hackstadt T (1996) Temporal analysis of the developing Chlamydia psittaci inclusion by use of fluorescence and electron microscopy. Infect Immun 64(10):4269–4278
26. Scidmore MA, Fischer ER, Hackstadt T (1996) Sphingolipids and glycoproteins are differentially trafficked to the Chlamydia trachomatis inclusion. J Cell Biol 134(2):363–374
27. Wolf K, Hackstadt T (2001) Sphingomyelin trafficking in Chlamydia pneumoniae-infected cells. Cell Microbiol 3(3):145–152
28. Roth AG et al (2009) Potent and Selective Inhibition of Acid Sphingomyelinase by Bisphosphonates. Angew Chem Int Ed 48(41):7560–7563
29. Kornhuber J et al (2010) Functional Inhibitors of Acid Sphingomyelinase (FIASMAs): A Novel Pharmacological Group of Drugs with Broad Clinical Applications. Cell Physiol Biochem 26(1):9–20
30. Geiger N et al (2022) The Acid Ceramidase Is a SARS-CoV-2 Host Factor. Cells 11(16):2532

31. Yasuda S et al (2001) A Novel Inhibitor of Ceramide Trafficking from the Endoplasmic Reticulum to the Site of Sphingomyelin Synthesis. J Biol Chem 276(47):43994–44002
32. Miyake Y et al (1995) Serine Palmitoyltransferase Is the Primary Target of a Sphingosine-like Immunosuppressant, ISP-1/Myriocin. Biochem Biophys Res Commun 211(2):396–403
33. Elojeimy S et al (2006) New insights on the use of desipramine as an inhibitor for acid ceramidase. FEBS Lett 580(19):4751–4756
34. Liu YY, Hill RA, Li YT (2013) Ceramide glycosylation catalyzed by glucosylceramide synthase and cancer drug resistance. Adv Cancer Res 117:59–89
35. Michel C et al (1997) Characterization of Ceramide Synthesis: A DIHYDROCERAMIDE DESATURASE INTRODUCES THE 4,5-TRANS-DOUBLE BOND OF SPHINGOSINE AT THE LEVEL OF DIHYDROCERAMIDE*. J Biol Chem 272(36):22432–22437
36. Koch-Edelmann S et al (2017) The cellular ceramide transport protein CERT promotes Chlamydia psittaci infection and controls bacterial sphingolipid uptake. Cell Microbiol, 19(10)
37. Chigorno V et al (2005) Sphingolipid Uptake by Cultured Cells: Complex Aggregates of Cell Sphingolipids with Serum Proteins and Lipoproteins Are Rapidly Catabolized. J Biol Chem 280(4):2668–2675
38. Sokoya T et al (2022) Pathogenic variants of sphingomyelin synthase SMS2 disrupt lipid landscapes in the secretory pathway. eLife 11:e79278
39. Niekamp P et al (2022) Ca(2+)-activated sphingomyelin scrambling and turnover mediate ESCRT-independent lysosomal repair. Nat Commun 13(1):1875
40. Wagner F et al (2026) Monitoring Sphingomyelin Biosynthesis at Nanoscale Resolution by Expansion Microscopy. bioRxiv, BIORXIV/2026/726241.
41. Rühling M et al (2025) A Novel Rapid Host Cell Entry Pathway Determines Intracellular Fate of Staphylococcus aureus. eLife Sciences Publications, Ltd.
42. Szperlinski M et al (2025) Obligate intracellular bacteria and host cell death pathways—the matter of life and death. Cell Tissue Res 402(3):413–439
43. Wilkerson BA, Argraves KM (2014) The role of sphingosine-1-phosphate in endothelial barrier function. Biochim Biophys Acta 1841(10):1403–1412
44. Proia RL, Hla T (2015) Emerging biology of sphingosine-1-phosphate: its role in pathogenesis and therapy. J Clin Invest 125(4):1379–1387
45. Bryan AM, Poeta MD (2018) Sphingosine-1-phosphate receptors and innate immunity. Cell Microbiol 20(5):e12836
46. Carr JM et al (2013) Sphingosine kinase 1 in viral infections. Rev Med Virol 23(2):73–84
47. Fohmann I et al (2023) Sphingosine kinase 1/S1P receptor signaling axis is essential for cellular uptake of Neisseria meningitidis in brain endothelial cells. PLoS Pathog 19(11):e1011842
48. Prakash H et al (2010) Sphingosine kinase-1 (SphK-1) regulates Mycobacterium smegmatis infection in macrophages. PLoS ONE 5(5):e10657

49. Van Brocklyn JR et al (1998) Dual actions of sphingosine-1-phosphate: extracellular through the Gi-coupled receptor Edg-1 and intracellular to regulate proliferation and survival. J Cell Biol 142(1):229–240
50. Collingro A et al (2011) Unity in Variety–The Pan-Genome of the Chlamydiae. Mol Biol Evol 28(12):3253–3270
51. Vieira CR et al (2010) Dihydrosphingomyelin impairs HIV-1 infection by rigidifying liquid-ordered membrane domains. Chem Biol 17(7):766–775
52. Scholz J et al (2025) Recruitment of the cellular lipid transport protein CERT to C. psittaci inclusions regulates the timing of bacterial egress. Sci Rep 15(1):18241
53. Hanada K, Sakai S, Kumagai K (2022) Natural Ligand-Mimetic and Nonmimetic Inhibitors of the Ceramide Transport Protein CERT. Int J Mol Sci, 23(4)
54. Kumagai K et al (2022) Chlamydial Infection-Dependent Synthesis of Sphingomyelin as a Novel Anti-Chlamydial Target of Ceramide Mimetic Compounds. Int J Mol Sci, 23(23)
55. Robertson DK et al (2009) Inclusion Biogenesis and Reactivation of Persistent Chlamydia trachomatis Requires Host Cell Sphingolipid Biosynthesis. PLoS Pathog 5(11):e1000664
56. van Ooij C et al (2000) Host cell-derived sphingolipids are required for the intracellular growth of Chlamydia trachomatis. Cell Microbiol 2(6):627–637
57. Beatty WL (2006) Trafficking from CD63-positive late endocytic multivesicular bodies is essential for intracellular development of Chlamydia trachomatis. J Cell Sci 119(Pt 2):350–359
58. Tachida Y et al (2020) Chlamydia trachomatis-infected human cells convert ceramide to sphingomyelin without sphingomyelin synthases 1 and 2. FEBS Lett 594(3):519–529
59. Tafesse FG et al (2007) Both sphingomyelin synthases SMS1 and SMS2 are required for sphingomyelin homeostasis and growth in human HeLa cells. J Biol Chem 282(24):17537–17547
60. Hackstadt T, Scidmore MA, Rockey DD (1995) Lipid metabolism in Chlamydia trachomatis-infected cells: directed trafficking of Golgi-derived sphingolipids to the chlamydial inclusion. Proc Natl Acad Sci U S A 92(11):4877–4881
61. Hörner EM et al (2025) Identification and characterization of a ubiquitin E3 RING ligase of the Chlamydia-like bacterium Simkania negevensis. PLoS Pathog 21(11):e1013626
62. Schindelin J et al (2012) Fiji: an open-source platform for biological-image analysis. Nat Methods 9(7):676–682
63. Wiznerowicz M, Trono D (2003) Conditional suppression of cellular genes: lentivirus vector-mediated drug-inducible RNA interference. J Virol 77(16):8957–8961
64. Krones D et al (2021) Staphylococcus aureus α-Toxin Induces Acid Sphingomyelinase Release From a Human Endothelial Cell Line. Front Microbiol 12:694489
65. Mühle C, Kornhuber J (2017) Assay to measure sphingomyelinase and ceramidase activities efficiently and safely. J Chromatogr A 1481:137–144

66. Livak KJ, Schmittgen TD (2001) Analysis of relative gene expression data using real-time quantitative PCR and the 2(-Delta Delta C(T)) Method. Methods 25(4):402–408
67. Jao CY et al (2009) *Metabolic labeling and direct imaging of choline phospholipids in vivo.* Proceedings of the National Academy of Sciences, 106(36): pp. 15332–15337
68. Rühling M et al (2024) Trifunctional sphingomyelin derivatives enable nanoscale resolution of sphingomyelin turnover in physiological and infection processes via expansion microscopy. Nat Commun 15(1):7456
69. Prell A et al (2024) The sphingosine kinase 2 inhibitors ABC294640 and K145 elevate (dihydro)sphingosine 1-phosphate levels in various cells. J Lipid Res 65(10):100631
70. Idkowiak J et al (2025) Best practices and tools in R and Python for statistical processing and visualization of lipidomics and metabolomics data. Nat Commun 16(1):8714

Figures

Figure 1

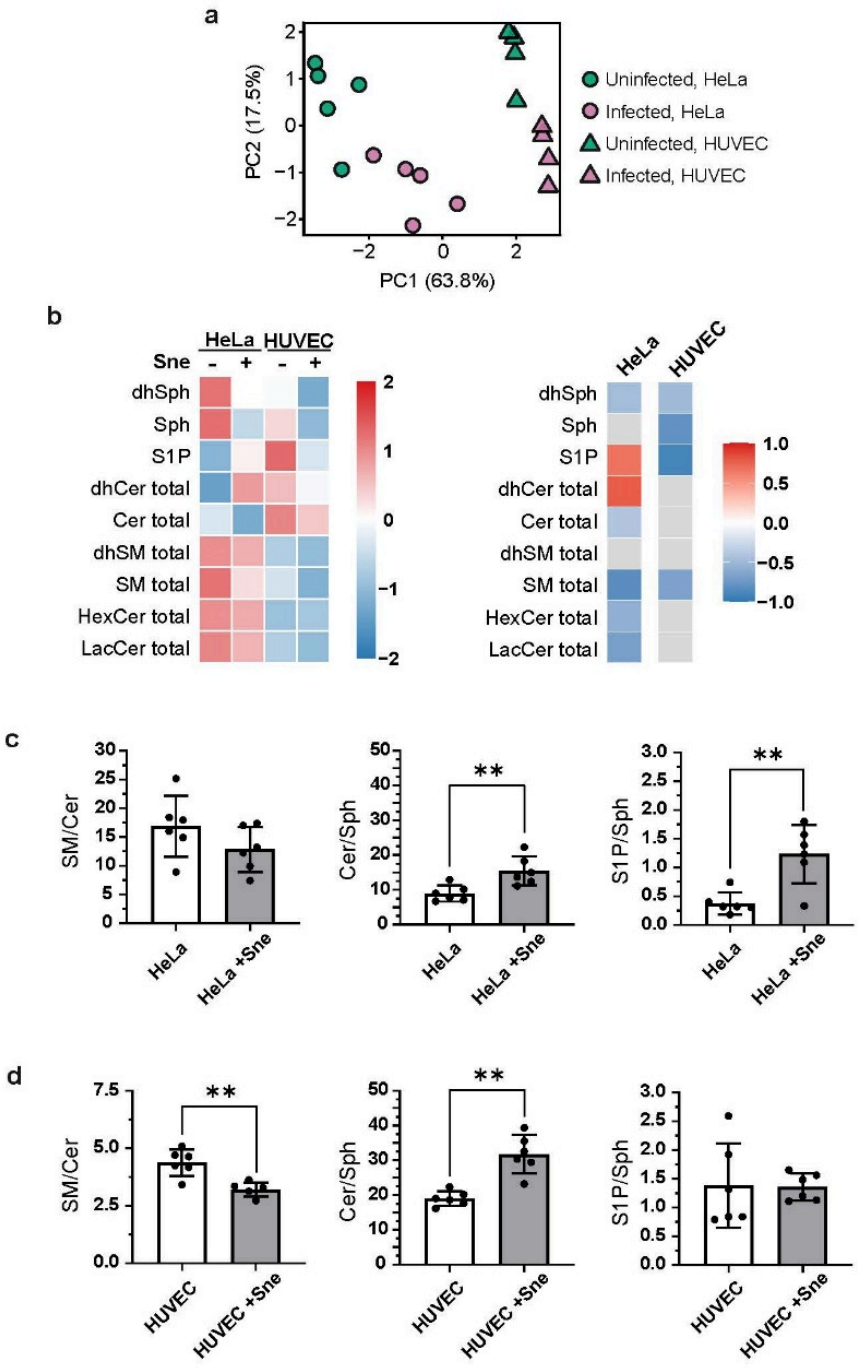


Figure 1

Sne infection remodels host sphingolipid metabolism. HeLa and HUVEC cells were infected with Sne for 3 or 2 days at an MOI of 1, respectively. Lipids were extracted with methanol and analyzed by LC-MS/MS. **(a)** Principal component analysis (PCA) of sphingolipid abundances (log_{10} (x+1)-transformed pmol/sample) in uninfected (green) and infected (purple) HeLa (n = 5) and HUVEC cells (n = 4). PCA was performed on mean-centered and unit-variance-scaled data. Samples segregate primarily by cell type

along PC1 (63.8 %) and by infection status along PC2 (17.5 %). **(b)** Left panel: z-scored heatmap of $\log_{10}(x+1)$-transformed pmol/sample values in uninfected (Sne -) and infected (Sne +) HeLa (n = 5) and HUVEC cells (n = 4). The heatmap shows how many standard deviations a data point is away from the mean across the row. Right panel: heatmap of differential sphingolipid abundances represented as $\log_2$ values derived from pairwise comparisons (infected – uninfected) with p-value adjusted for False-Discovery Rate (FDR). Values are displayed ranging from blue (decrease) to red (increase), with white indicating no change. Non-significant comparisons (FDR ≥ 0.05) are masked (grey). **(c, d)** Quantification of sphingolipid ratios (SM/Cer, Cer/Sph, S1P/Sph) in uninfected (white) and infected (grey) HeLa (c) and HUVEC (d) cells. Graphs represent mean ± SD (n=6). Statistical significance was assessed using a one-sample t-test and a Wilcoxon test. *p < 0.05; **p < 0.01; ns, not significant.

Figure 2

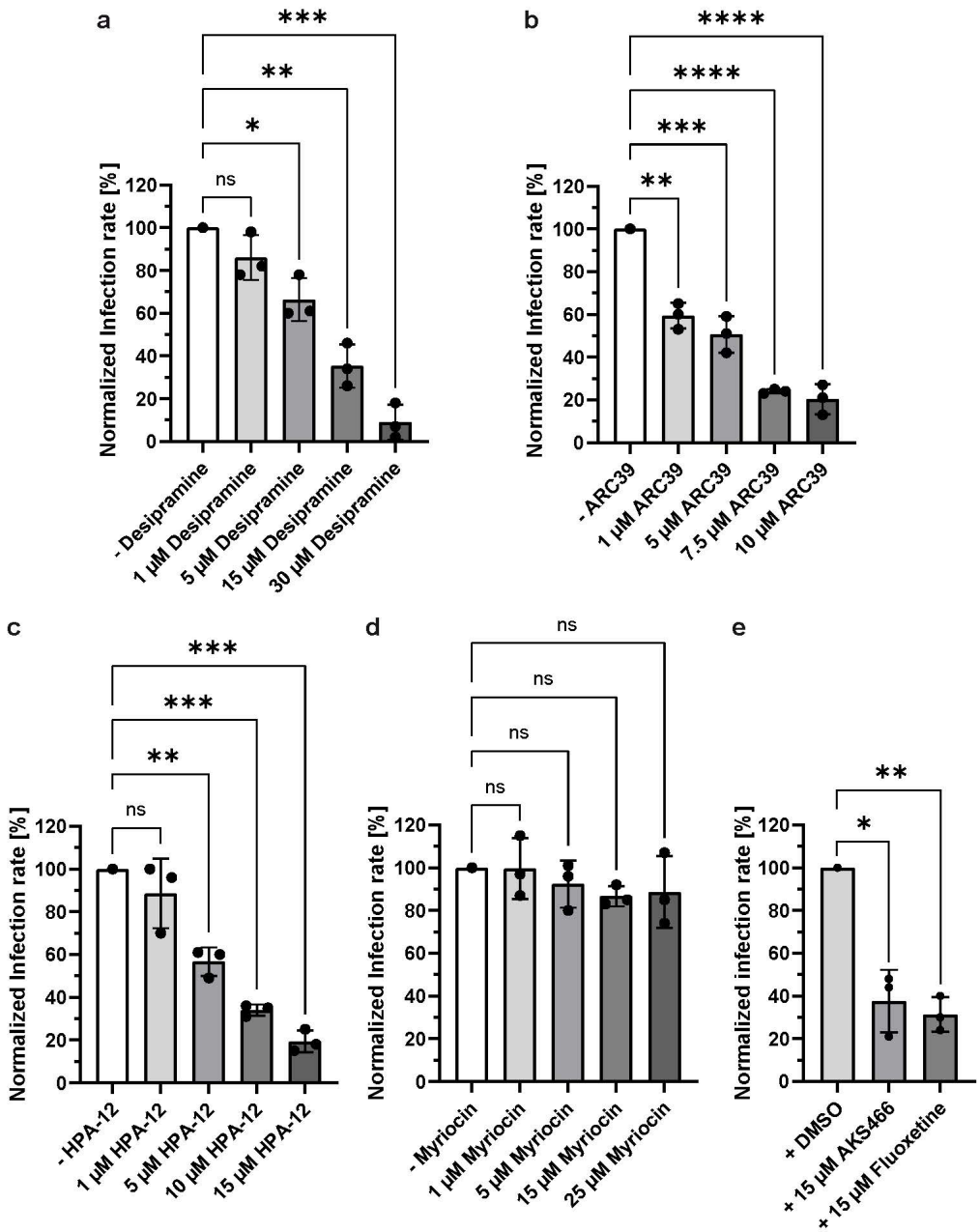


Figure 2

Inhibitors of sphingolipid metabolism affect Sne infection in a dose-dependent manner. (a-e) Cells were pre-treated for 3 h with desipramine (1-30 µM, a), ARC39 (1-10 µM, b), HPA-12 (1-15 µM, c), myriocin (1-25 µM, d), and 15 µM AKS466 or fluoxetine (e) before infection with Sne at an MOI of 1. Infection rates (infected/total cells) were determined by fixing and staining of infected cells 72 h p.i. using antibodies against SnGroEL and DAPI, followed by microscopy. At least 100 cells per sample were

counted, and the percentage of infected cells was normalized to that of the corresponding vehicle control (white). The graphs represent mean ± SD (n = 3). Statistical significance was assessed using a one-sample t-test and a Wilcoxon test. *p < 0.05; **p < 0.01; ns, not significant.

Figure 3

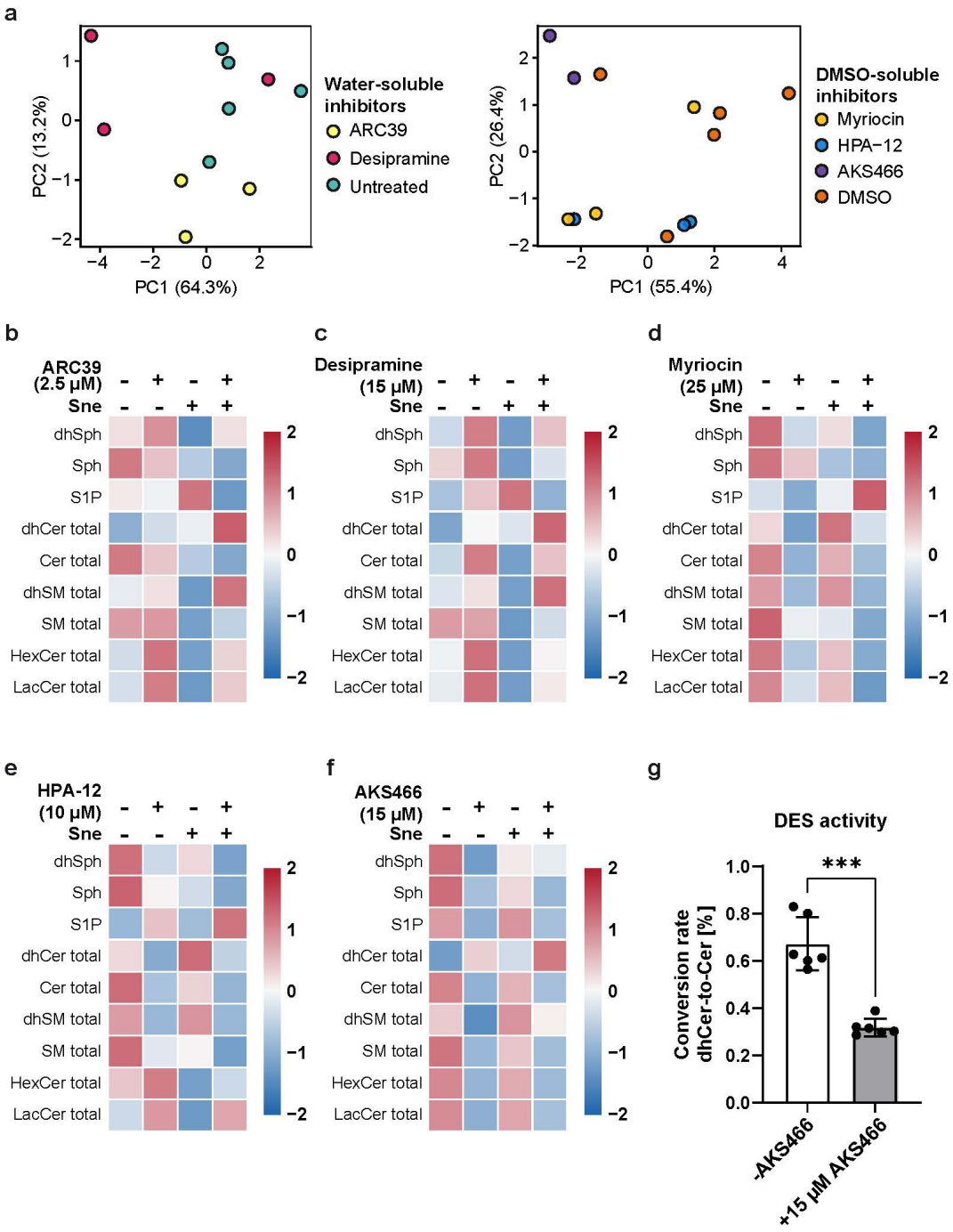


Figure 3

Sne reshapes the host sphingolipidome under inhibitor treatment. HeLa cells were treated with sphingolipid pathway inhibitors and infected as described in Fig. 2. Lipids were extracted with methanol and analyzed by LC-MS/MS. **(a)** PCA of sphingolipid abundances from uninfected HeLa cells (log_{10} (x+1)-transformed pmol/sample) treated with water-soluble ASM inhibitors (left panel) or DMSO-soluble inhibitors (right panel) was performed on mean-centered and unit-variance-scaled data. Water-soluble inhibitor ARC39- and desipramine-treated cells show separation primarily along PC1 (64.3 %) and PC2 (13.2 %). DMSO-soluble myriocin-, HPA-12-, and AKS466-treated cells separate along PC1 (55.4 %) and PC2 (26.4 %). Circles represent individual biological replicates, and colors indicate the inhibitor used. **(b-f)** Heatmaps showing absolute sphingolipid abundances (log_{10} (x+1)-transformed pmol/sample, z-scored) in ARC39- (b, n = 3), desipramine- (c, n = 3), myriocin- (d, n = 3), HPA-12- (e, n = 3), and AKS466- (f, n = 2) treated cells and controls (untreated or DMSO, n = 5 for both) when left uninfected (Sne -) or when infected (Sne +). Values are displayed ranging from blue (decrease) to red (increase), with white indicating no change. **(g)** Quantification of DES activity (conversion rate of dihydroceramide to ceramide) in HeLa cells treated with 15 µM AKS466 compared to untreated cells (- AKS466). The graph represents mean ± SD (n = 6). Statistical significance was determined by an unpaired two-tailed t-test ($p < 0.001$).

Figure 4

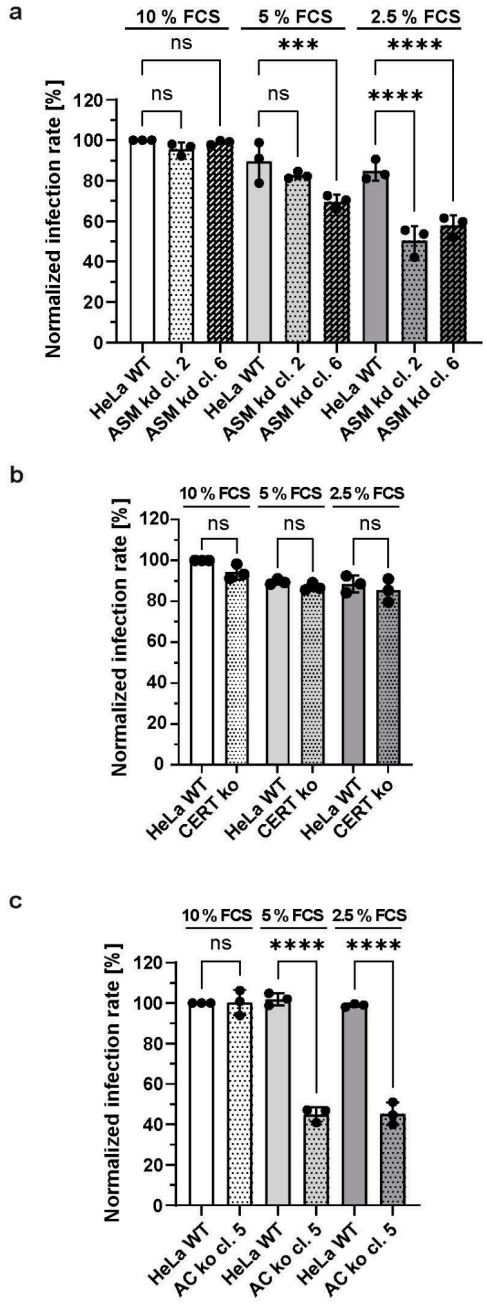


Figure 4

Sne infection depends on ASM and AC, but not CERT. (a-c) HeLa parental WT cell line (HeLa WT) and a cell line with a knockdown of acid sphingomyelinase (ASM kd, a), a knockout of ceramide transfer protein (CERT ko, b), or a knockout of acid sphingomyelinase (AC ko, c) were maintained under standard (10 % FCS) or reduced serum conditions (5 % and 2.5 % FCS). Cells were infected with Sne at an MOI of 1, fixed at day 3 p.i., and immunostained with antibodies against SnGroEL. Cell nuclei were visualized by

DAPI staining. The percentage of infected cells was determined and normalized as in Fig. 2. The graphs show mean ± SD (n = 3). Statistical significance was determined using one-way ANOVA followed by Šídák's multiple comparisons test. *p ≤ 0.05; **p ≤ 0.01; ***p ≤ 0.001; ****p ≤ 0.0001; ns, not significant.

Figure 5

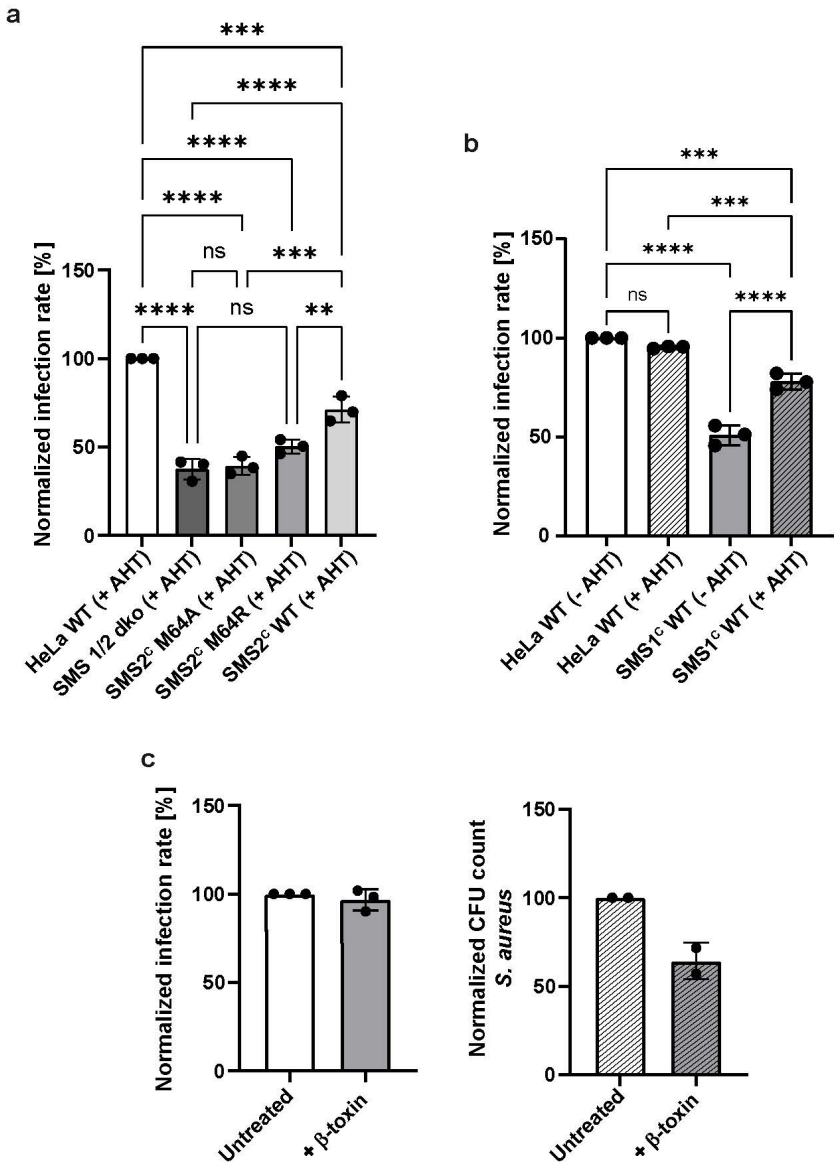


Figure 5

Sne infection depends on host sphingomyelin synthase activity. (a, b) Parental HeLa cell line, a cell line with a knockout of sphingomyelin synthase 1 and 2 (SMS1/2 dko), or the SMS1/2 dko cell line complemented with anhydrotetracycline (AHT)-inducible constructs for expression of wild type SMS2 enzyme ($SMS2^c$ WT), mutated SMS2 enzyme that is directed to endoplasmic reticulum ($SMS2\text{-}M64A^c$), or wild type SMS1 enzyme ($SMS1^c$ WT) were infected with Sne at an MOI of 1. Infection rates were quantified 72 hours p.i. as described for Fig. 2. The graphs represent mean ± SD (n = 3). Statistical significance was determined using one-way ANOVA followed by Šídák's multiple comparisons test. *p ≤ 0.05; **p ≤ 0.01; ***p ≤ 0.001; ****p ≤ 0.0001; ns, not significant. **(c)** Infection rates determined as in a and b in HeLa cells treated with 100 ng/mL β-toxin for 75 min before Sne infection (left panel, n = 3). Positive control using *Staphylococcus aureus*, where colony-forming units (CFU) were quantified following β-toxin treatment and normalized to that of the untreated control (right panel, n = 2).

Figure 6

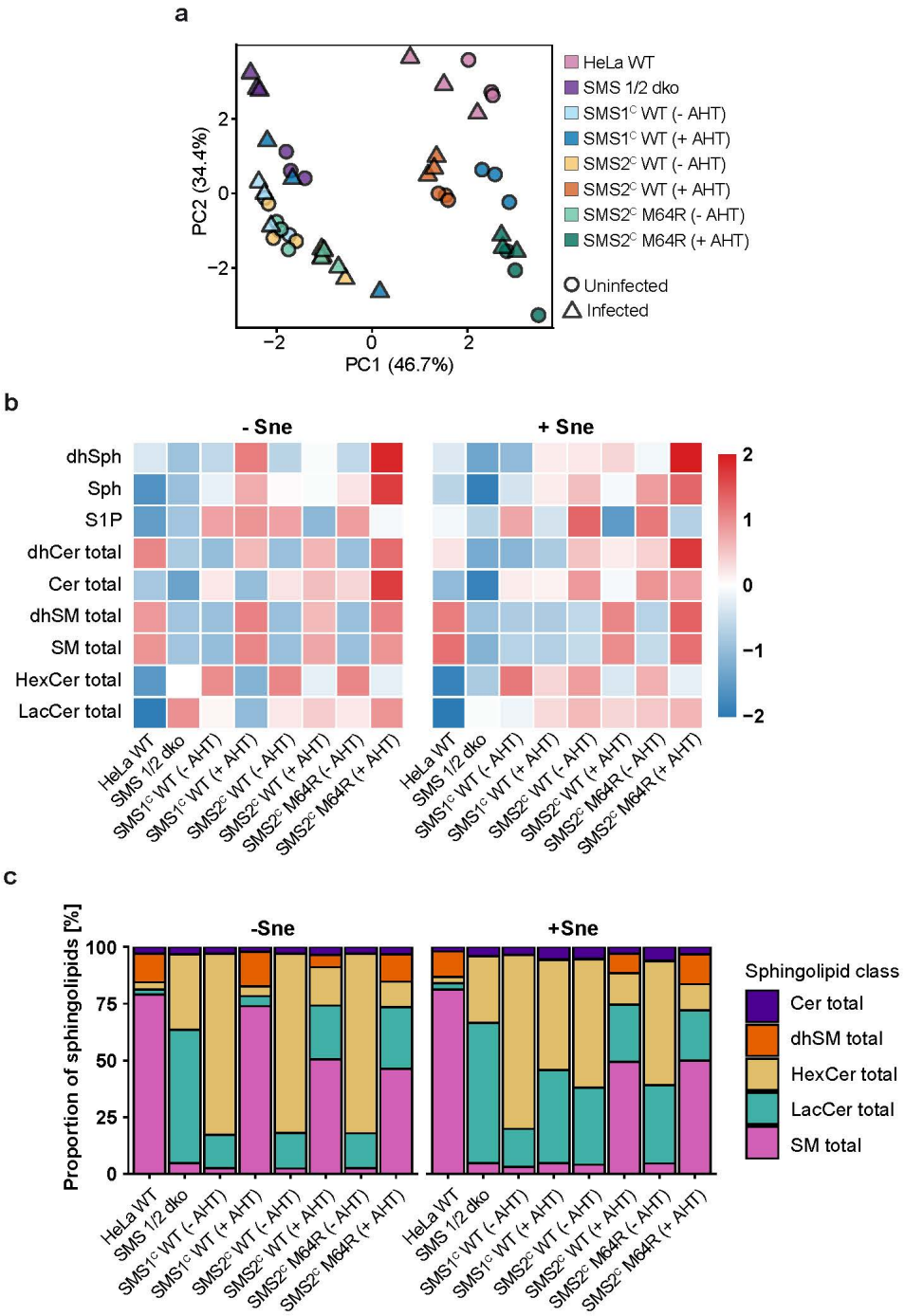


Figure 6

Sne infection alters host SM-Cer balance in an SMS-dependent manner. (a) PCA analysis of sphingolipid abundances was performed on mean-centered and unit-variance-scaled data (log_{10} (x+1)-transformed pmol/sample) across SMS1/2 genotypes described in Fig. 5 (HeLa WT, SMS1/2 dko, SMS1^{C} WT (-/+AHT), SMS2^{C} WT (-/+AHT), and SMS2-M64R^{C} (-/+AHT), in uninfected (circle) and infected (triangle) cells (n = 3). Samples segregated along PC1 (46.7 %) and PC2 (34.4 %), showing differences

associated with SMS genotype under AHT induction and infection status. Colors denote SMS genotype and shapes indicate infection status. **(b)** Heatmap showing absolute sphingolipid abundances (log_{10} (x+1)-transformed pmol/sample, z-scored, across each row representing a sphingolipid class) in cell lines described in Fig. 5 with (+ Sne) and without (- Sne) infection. **(c)** Relative distribution of sphingolipids in SMS-modified cell lines under uninfected (-Sne) and infected (+Sne) conditions. Stacked bar plots showed the proportion of total sphingolipid classes, including ceramides (Cer), dihydrosphingomyelin (dhSM), hexosylceramides (HexCer), lactosylceramides (LacCer), and sphingomyelin (SM), within the total sphingolipid pool.

Supplementary Files

This is a list of supplementary files associated with this preprint. Click to download.

- 5.SourceData.xlsx
- SupplementaryInformationFinal.pdf